12, 449 (1964).
[21]P. Brix and G. Herzberg, Can. J. Phys. 29, 294 (1958).
[22]L. M. Branscomb, D. S. Burch, S. J. Smith, and S. Geltman, Phys. Rev. 111, 504 (1958).
[23]G. S. Hurst, L. B. O'Kelly, and T. E. Bortner, Phys. Rev. 123, 1715 (1961).
[24]The form of Eq. (2) is not altered by the effect of the finite energy spread of the electron beam. The coefficients $a_{L,|\mu|}$, however, must be averaged over all electron energies and referred to a mean value of electron momentum given by $\bar{k} = \int kf(k)\,dk / \int f(k)\,dk$, where $f(k)$ is the electron-momentum distribution function. The electron energy spread was found to be about 0.3 eV, and the stated values for the electron energy correspond to $\bar{k}$.
[25]R. de L. Kronig, Z. Physik 50, 347 (1928).
[26]G. Herzberg, *Spectra of Diatomic Molecules* (Van Nostrand, Princeton, N. J., 1950), p. 283.
[27]T. F. O'Malley, Phys. Rev. 150, 14 (1966).

PHYSICAL REVIEW A VOLUME 2, NUMBER 5 NOVEMBER 1970

Absolute Measurement of Differential Cross Sections for Electron Scattering in Helium†

G. E. Chamberlain,* S. R. Mielczarek, and C. E. Kuyatt
National Bureau of Standards, Washington, D. C. 20234
(Received 29 July 1969; revised manuscript received 22 June 1970)

Absolute measurements of cross sections for electron-impact scattering in helium at an angle of 5° have been made for elastic scattering and excitation of the $2\,^1P$ and $2\,^1S$ states and for incident energies of 50–400 eV. Cross-section values of $\sigma(2\,^1P, 5°)$ are found to be lower than theoretical Born values by (9.5 ± 5.4)% at 400 eV, (31.5 ± 4.6)% at 100 eV, and (62.5 ± 3.4)% at 50 eV. Deduced values of total $2\,^1P$ excitation cross sections ($E \geq 100$ eV) are in agreement with other experimental values. Our measurements for elastic scattering agree well with recent theoretical calculations.

I. INTRODUCTION

This article reports the absolute[1] measurement of small-angle differential cross sections for electron-impact scattering from He. Measurements were carried out for elastic scattering and excitation of the $2\,^1P$ and $2\,^1S$ states at fixed angles of 5° for incident energies of 50–400 eV utilizing a high-resolution electron spectrometer with a static gas target. The principal motivation for this work was (a) to provide accurate absolute small-angle cross-section values for normalization of angular-distribution measurements and (b) to study the nature and degree of breakdown of the Born approximation for excitation of the (optically) allowed $2\,^1P$ state.

Until recently,[2] little work appears to have been done on the absolute determinations of differential cross sections for electron scattering in He at small angles (< 15°) and in the energy range of 1–1000 eV.[3] Lawson *et al.*,[4] in determining theoretical zero-angle cross sections for He, pointed out inconsistencies existing in experimental data and emphasized the need for accurate small-angle elastic cross sections. It is desirable, also, to have accurate inelastic cross sections at small angles, where the contribution to the total cross section is the most significant. Excellent work on angular distributions in various gases has been carried out by Lassettre and collaborators[5–7] who normalized He ($2\,^1P$) excitation to theoretical Born values in order to calibrate their apparatus.

Although it is doubtful that the Born approximation is valid for excitation at 50 eV, evidence has been reported that the Born approximation still applies within a few percent down to 100 eV for differential[8] and total[9] $n\,^1P$ excitations, whereas significant deviations from Born occur at 1500 eV for total[9] $n\,^1S$ excitations. In contrast, we find the difference between this experiment and Born theory for $2\,^1P$ excitation to be (9.5 ± 5.4)% at 400 eV and (31.5 ± 4.6)% at 100 eV.

In Sec. II, we briefly describe the apparatus. Section III discusses the theory of the experiment, the methods used in obtaining experimental parameters, and calibration and consistency checks made on the apparatus. In Sec. V, analysis of the data is discussed, the results are presented, and sources of systematic error are considered. In Sec. VI, we compare our results to other values of experimental and theoretical cross sections selected from various authors.

II. APPARATUS

Except for minor modifications, the apparatus has been described in detail by Kuyatt and Simpson.[10,11] It was designed to operate over the energy range 50–400 eV with a resolution range of 0.04 to 0.1 eV. In the interest of completeness, we

review here the salient features of the electron spectrometer and discuss an additional important component – the pressure measuring instrumentation.

Figure 1 shows, in detail, the sizes and spacing of all lenses and apertures as actually used in the present apparatus. The spectrometer is divided into two parts, a rotatable monochromator to collimate the incident electron beam in energy and space and an analyzer to select in energy and space, electrons that have scattered within the flexible stainless-steel bellows chamber connecting these

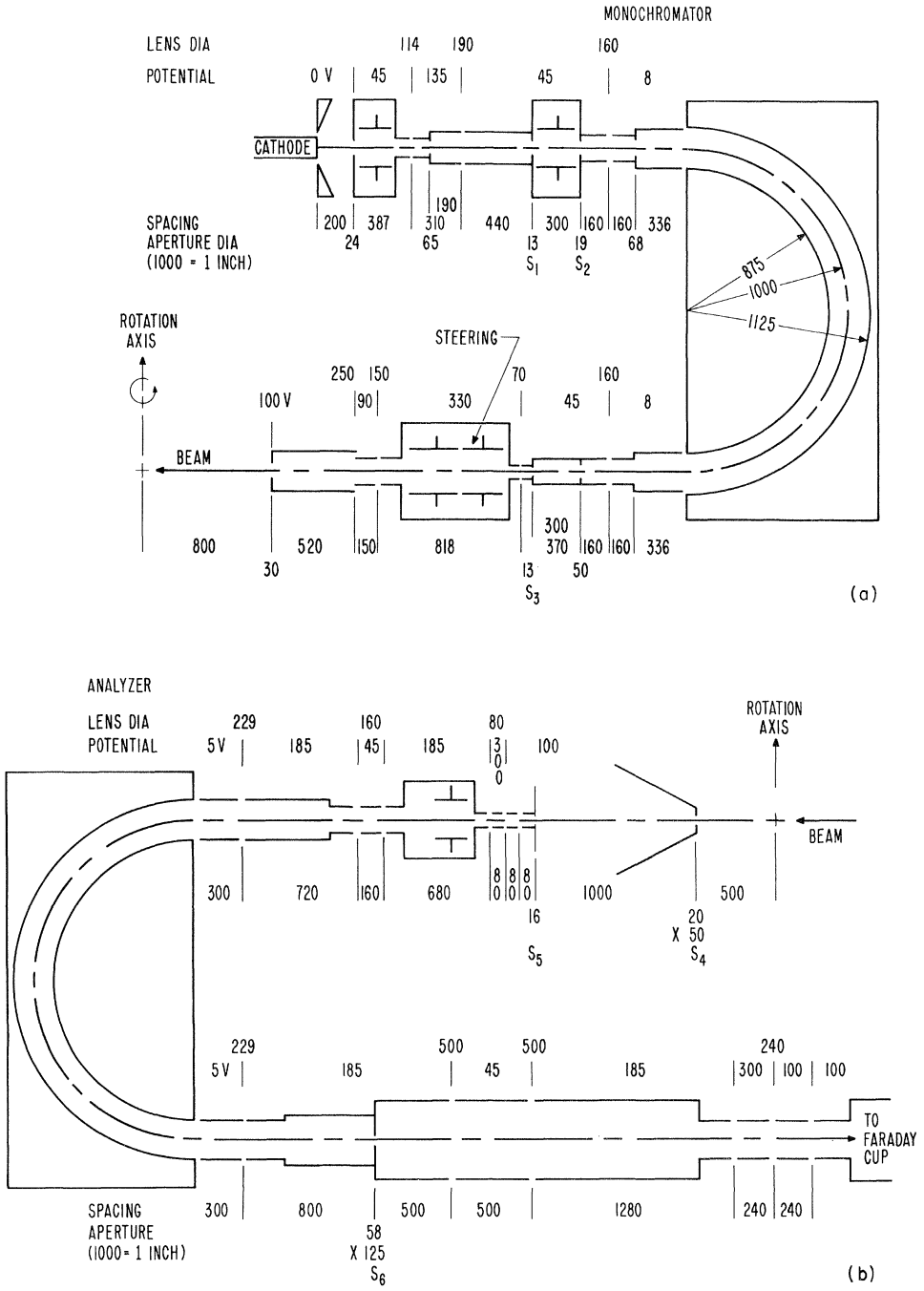

FIG. 1. Schematic of electron spectrometer showing lens diameters, positions of lens gaps and apertures, and typical operating voltage for 100-eV impact energy and over-all resolution of 0.12 V. In the low-resolution mode the mean energy of the analyzer was 21 eV and the over-all resolution was 0.6 eV.

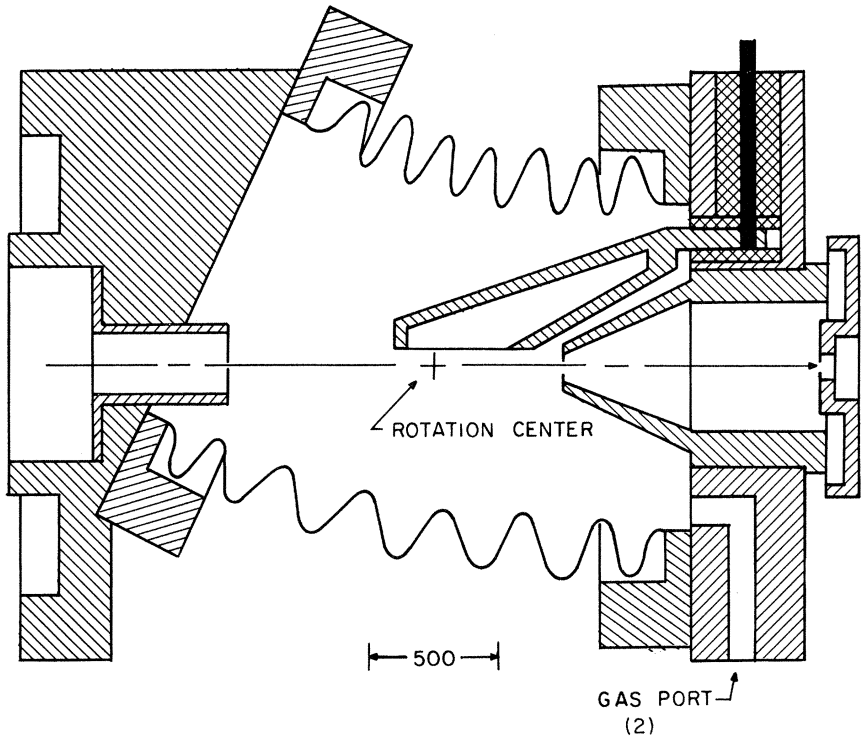

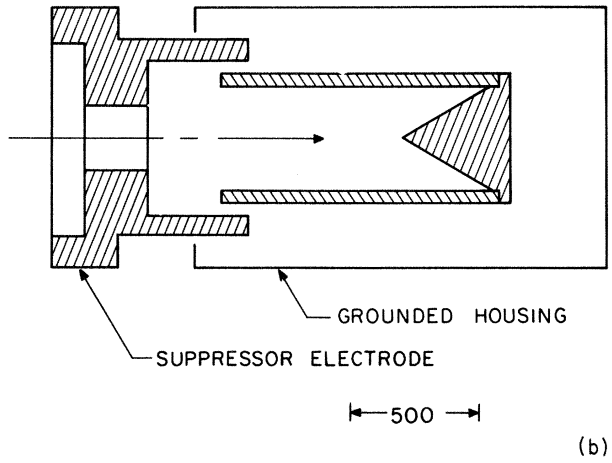

FIG. 2. Details of (a) scattering chamber and Faraday collector, (b) analyzer detector. Dimensions are in 0.001 in.

two parts. Hemispherical electrostatic deflectors were used for energy dispersion. All lenses and the dispersing elements were made of copper, and beam defining apertures were of 0.005-in.-thick Mo. The rest of the support pieces and vacuum housing were of type-304 stainless steel.

The pump chain consisted of a rotary mechanical pump, zeolite trap, mercury diffusion pump, refrigerated baffle, and liquid-nitrogen trap. Moderate bakeout of the apparatus up to 300 °C was sufficient for stable operation. A typical background pressure of 2×10^{-8} Torr was achieved when no gas was flowing into the system.

Research-grade He was admitted to the target cell from an all-metal gas-handling system and pumped out through the scattering chamber apertures. The ratio of pressure inside the cell to that at the vacuum-chamber ion gauge was ~1000:1. The regions outside the chamber were as open as possible to minimize local increases in pressure.

Details of the target chamber, target-chamber Faraday cup, and analyzer Faraday cup are shown in Fig. 2. Current measurement and collector efficiency are discussed below.

Except as noted, electrode voltages were supplied directly by low-impedance (0.01-Ω) voltage sup-

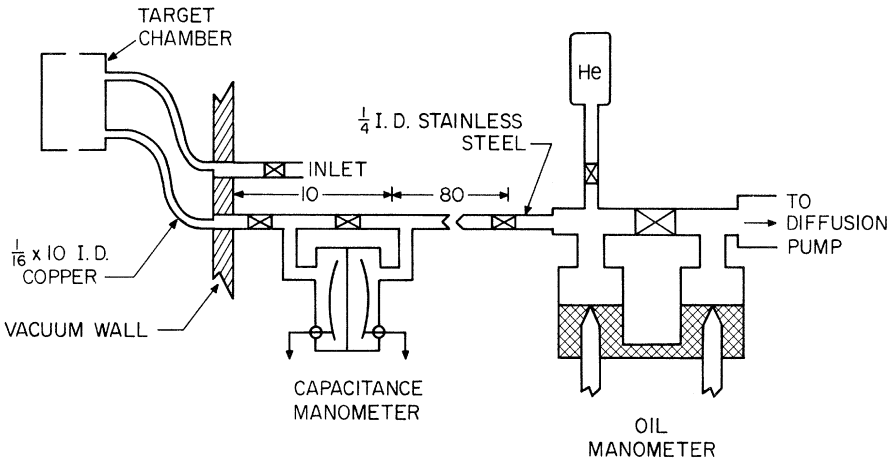

FIG. 3. Schematic of pressure measuring apparatus. Dimensions are in inches and are illustrative (about 20% accuracy).

plies. Deflecting electrode voltages were derived from 10 K potentiometers across regulated voltage supplies. The mean and deflecting potentials of the hemispheres were obtained from potentiometers across mercury battery sources. Some noncritical potentials were provided by potentiometers and dry-cell batteries. All electrical leads were rf bypassed at the vacuum feedthrough.

The dc magnetic field in the laboratory was reduced to less than 50 mG by a single pair of Helmholtz coils appropriately oriented. There was no necessity to shield against ac magnetic fields.

The angular drive had two stages of gear reduction: a commercial vacuum-tight rotary feedthrough of the "harmonic drive" type (78:1 ratio), and an internal pair of precision spur gears (4:1). The final 4-in.-diam gear was an integral part of the monochromator bench.

Pressure measurement was made with a micrometer-point-contact oil manometer connected to the target cell by a static transfer tube. To prevent oil contamination of the spectrometer, the transfer line was divided into two parts by a commercial metal-diaphragm capacitance-type manometer with a sensitivity of 0.01–1000 mTorr. The oil manometer was constructed in the NBS machine shop following the design developed by the NBS Vacuum Measurements Section.[12] The copper tubulation between the target chamber and vacuum wall was $\simeq$1.5 mm i.d. Figure 3 illustrates the arrangement for measuring pressure.

III. EXPERIMENTAL ARRANGEMENT

A. Theory

1. *Pressure Dependence of Scattered Current*

Differential cross sections were determined by observing scattering from an electron beam traversing a gas target. The differential cross section $\sigma(W, \theta)$ for a discrete energy loss W is defined as the scattering yield per unit solid angle and per atom for deflection through an angle θ. Essential features of the methods used in determining cross sections from scattering in a static gas target are reviewed by Kuyatt.[13]

If the scattered current leaving the target through the exit apertures consists primarily of electrons that have scattered only once, then the relationship between the exit current I and the cross section σ is

$$I = I_0 \sigma(W, \theta)(l\Delta\Omega)_{\text{eff}}\, n e^{-n/n_0}, \tag{1}$$

where I_0 is the current incident on the target gas, n is the target density, $(l\Delta\Omega)_{\text{eff}}$ is an effective product of path length and solid angle, and n_0 is a beam attenuation constant.

The dependence on pressure, or number density, shown in Eq. (1) has been derived in detail by Lassettre.[14] The exponential attenuation factor is due to the removal of particles from the incident and scattered beam by the totality of all scattering processes. However, $(1/n_0)$ cannot be simply calculated as the product of total cross section and target thickness, since the amount of compensation[15] is unknown. Compensation arises from replacement of electrons scattered out of the beam by electrons scattered into it from regions adjacent to the geometrically defined beam paths. Exponential attenuation in the present apparatus has been demonstrated previously,[16] and the attenuation constant n_0 was found to be invariant for elastic and $2\,^1P$ scattering at 5° and for $2\,^1P$ scattering at 0°. This invariance was maintained for attenuations of over 90%. In the present experiment, beam attenuations of 5 to 25% occurred for pressures of 10 to 40 mTorr. The attenuation constant n_0 is not to be confused with the constant μ discussed below and used in the least-squares fitting of the data (μ is about 30% larger than $1/n_0$).

With low or moderate beam attenuations, the

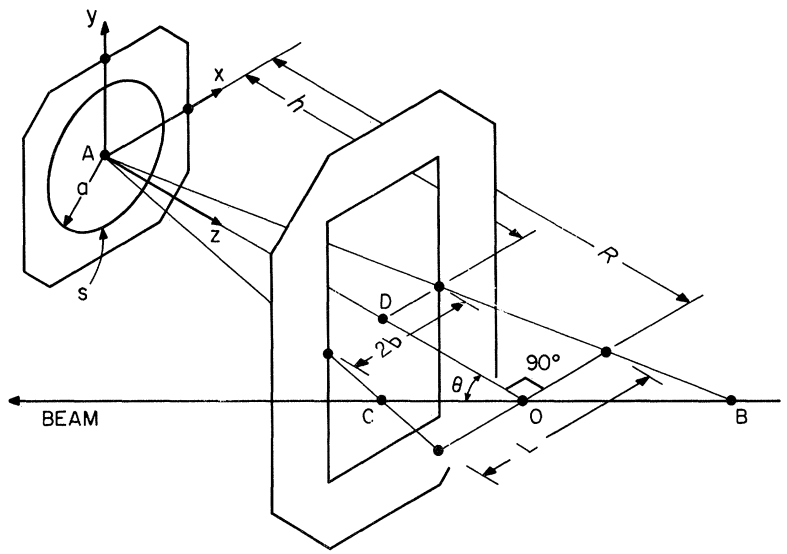

FIG. 4. Schematic of the scattering geometry showing notations used in the text. The slit at D and the aperture at A correspond to apertures S_4 and S_5 in Fig. 1.

exponential dependence on density can reasonably be assumed to be valid, but under unfavorable conditions plural scattering may cause an undesirable amount of additional scattering signal. An example presented in Ref. 16 shows that for $2\,^1P$ scattering at 400 eV for angles greater than 10°, there is a significant contribution from the double process of large-angle elastic scattering plus small-angle inelastic scattering. The contribution from plural scattering is negligible at 5°, not only for the case of 400 eV given in Ref. 16 but also at lower incident energies. It is clear from the evidence in Ref. 16 and the results of the present data analysis that Eq. (1) is a valid model for predicting the observed scattered current in terms of the experimental parameters. The application of Eq. (1) to the experimental data is described in Sec. V.

2. *Scattering Geometry*

Figure 4 illustrates the slit-aperture scattering geometry for an idealized very narrow beam. Geometric dimensions for the present experiment are listed in Table I. The contribution of particles to the detected scattered current from each element of beam path is proportional to the solid angle available for these particles to reach the exit aperture at A in Fig. 4. It is necessary to define an effective product of path length and solid angle $(l\Delta\Omega)_{\text{eff}}$, as introduced in Eq. (1), because the solid angle is not constant over the path length that contributes to the observed scattering, and in fact, the solid angle drops to zero at the ends of the path length. In addition, in considering higher-order corrections for finite angular resolution, the change of cross section with angle must be taken into account.

TABLE I. Scattering geometry parameters.

Item	Value
$2b$	0.502 (5) mm [a]
$2a$	0.399 (4) mm
R	3.80 (2) cm
h	2.56 (2) cm
$L\Omega$	0.0644 (19) μmsr

[a]Errors in the last significant figures are given in parentheses and are estimated limits of error (see Sec. III B 5).

Several papers[17] on high-energy proton-proton scattering contain a detailed analysis of higher-order corrections to the expected scattered intensity in a gas target. The work of Breit *et al.* treats the general case of a slit-aperture scattering geometry and discusses the effects of beam size and divergence. However, there were errors in the cross-section-independent terms that were corrected in both of the latter papers. Critchfield and Dodder restrict their treatment to the case of a slit-hole scattering geometry, but include easily evaluated terms that are related to the beam size and divergence. The calculations of Silverstein include, possibly for the first time, the case of a hole-hole scattering geometry.

We present here the procedure taken from Ref. 17 for evaluating $(l\Delta\Omega)_{\text{eff}}$ when the incident beam is very narrow. In Fig. 4, the y axis is parallel to the slit edge, the x axis perpendicular to it, and the yz plane passes midway between the slit edges. The z axis passes through the center of the exit aperture at A, the slit plane at D, and intersects the beam at 0. The incident beam is assumed to coincide with the z axis at zero angle. The correction terms include values of x, x^2, and y^2 averaged over the exit aperture as well as $\sigma'(\theta)$ and $\sigma''(\theta)$,

the first and second derivatives with respect to the angle of the cross section. By maintaining good apparatus alignment and averaging observations at symmetric values of θ, the terms in $(x)_{av}$ can be omitted. For a circular aperture of radius a, $(x^2)_{av} = (y^2)_{av} = \frac{1}{4}a^2$. With the above restrictions, the effective product of path length and solid angle for a slit-round-hole system is

$$(l\Delta\Omega)_{eff} = (L\Omega/\sin\theta)(1+\eta), \tag{2a}$$

where

$$\eta = \frac{a^2}{4}\left(\frac{1}{R^2}(\cot^2\theta - \tfrac{3}{2}) - \frac{3}{2h^2}\right)\frac{b^2}{2h^2} + \frac{\sigma'(\theta)}{\sigma(\theta)}\frac{a^2}{R}\cot\theta\left(\frac{1}{8R} - \frac{1}{4h}\right)$$

$$+\frac{\sigma''(\theta)}{\sigma(\theta)}\left(\frac{b^2}{6h^2} + \frac{a^2}{8h^2}\right). \tag{2b}$$

Note that to first-order terms in the geometry and provided symmetric angular observations are averaged,[18] the effective product of path length and solid angle is given by

$$(l\Delta\Omega)_{eff} = L\Omega/\sin\theta,$$

where θ is the nominal angle of scattering, L is the width of the field of view at the scattering center seen by an observer at the center of the exit aperture ($L = 2bR/h$), and Ω is the solid angle subtended at the scattering center by the exit aperture ($\Omega = S/R^2$, where S is the area of the aperture).

Contributions to η due to beam size and divergence were negligible for the present experiment. The most significant term in Eq. (2) was the last term which was $2.35\times10^{-4}\sigma''(\theta)/\sigma(\theta)$ for the present apparatus. Even then, corrections were necessary only for the rapidly falling $2\,^1P$ cross section at incident energies of 150 eV and above. The curvature was calculated from an analytic approximation for $\sigma(2\,^1P, \theta)$ and checked experimentally. The analytic expression used was

$$\tfrac{1}{2}[W(P_1/P_2)K^2]\sigma(2\,^1P, \theta) = f_0(1+x)^{-6} \tag{3}$$

in atomic units, where W is the energy loss, P_1 and P_2 are the incident and final momentum, K is the momentum transfer, $x = K^2/\alpha^2$, and α^2 and f_0 are constants. The left-hand side of Eq. (3) is the apparent generalized oscillator strength,[19] and the right-hand side is an analytic approximation similar to that introduced by Lassettre[20] and extended by Vriens.[21] Over the range $0.2 < K^2 < 1.0$, the experimental dependence[6,8] on angle of $\sigma(2\,^1P, \theta)$ is bound by the Born-like dependence (Sec. VI A) which can be approximated by setting $\alpha^2 = 3.68$ in Eq. (3), and the hydrogenlike dependence which is given[21] by $\alpha^2 = 3.39$. The change in η for the above range in α^2 is 0.2% at 400 eV.

3. *Analyzer*

The analyzer serves two functions: (a) resolution of the electrons that have lost a specified amount of energy in the target from all other electrons, and (b) transmission to the detector and detection of a known fraction of the electrons leaving the collision-chamber exit hole. This fraction defines the efficiency of the analyzer.

The beam transport optics were designed to ensure no loss of electrons to the lenses or deflecting hemispheres and, consequently, had a very open structure, as seen in Fig. 1. The effective entrance aperture to the hemispheres is the image of the aperture S_5 onto the entrance plane; the effective exit slit is the image of the real slit S_6. The slit S_6 is the only place between S_5 and the analyzer Faraday cup where electrons can properly be lost. It is convenient to distinguish two modes of operating the analyzer when observing a resolved energy-loss peak.

In the high-resolution mode there is a sufficient dispersion in the analyzer to remove some of the electrons within a loss peak[22] at the slit S_6. Assuming no loss of electrons between S_5 and S_6, the analyzer and detector can be calibrated in the following manner. Rudd and Kuyatt[23] have shown that for a resolved peak in which the spatial and angular characteristics at the analyzer entrance plane do not depend on energy; the total current into the analyzer I_{in} is related to the current $I_{out}(E)$ arriving at the detector by

$$\Delta E_{eff} I_{in} = \int_E I_{out}(E)\,dE, \tag{4}$$

where ΔE_{eff} is a geometric constant of the analyzer and E is the mean energy loss. ΔE_{eff} can be calibrated by measuring the area under a convenient peak, such as the incident beam, and the current I_{in}.

The analyzer spheres themselves made an efficient detector for measuring I_{in} when the primary beam was used as the source of current. By increasing the deflecting voltage, the beam was collected on the inner sphere and the accelerating field prevented low-energy secondaries from escaping. In addition, by measuring the current to both inner and outer spheres, the small fraction of elastically reflected secondaries were accounted for. Background was conveniently measured by biasing the collector in the target chamber to prevent the primary beam from entering the analyzer.

A 100% transmission mode of operating the analyzer was obtained by increasing the analyzing energy to about 20 eV and, at the same time, altering the lens voltages so that the beam entering the analyzer was demagnified and made smaller than the exit slit of the analyzer. The energy pass band was flat topped (less than 0.5% change in intensity) for 0.24 eV and had a base width of 1.2 eV. Under these conditions, the intensity of the center of the $2\,^1S$ loss peak was free of contribution from the

tail of the much stronger $2\,^1P$ loss peak. The full transmission mode made the measurement of scattered current easier and more reliable; therefore, this mode was used, except for a few early measurements in the high-resolution mode.

4. *Monochromator*

The energy-selecting hemispheres of the monochromator section were identical to those of the analyzer and did not have physical slits in the entrance and exit plane. The advantages of this system have been discussed earlier.[10] The electron beam was initially defined by apertures S_1 and S_2 in the gun leg, and the corresponding size and divergence (maximum angle with respect to central ray) at the scattering center were predicted by ray-tracing calculations.[24] Incident beam parameters are given in Table II.

We have found lens design by ray tracing to be reliable to about 10% when space-charge effects are negligible. Space-charge effects in the monochromator are currently being investigated in this laboratory and are believed to be responsible for the observed beam divergence being considerably less than the calculated divergence of about 1°. To first order, the estimate of divergence from the angular profile is independent of beam diameter at the scattering center, if the beam size is less than the width $(2bR/h)$ of acceptance of the analyzer. This criterion is satisfied by the nominal beam size given in Table II. The actual diameter of the beam at the scattering center is not expected to be seriously larger than predicted since, in order to maximize the current to the analyzer when aligning the beam, it is necessary to produce a converging beam that enters the scattering chamber through a 0.03-in.-diam hole.

5. *Incident Current*

The current I_0 incident upon the target gas was measured by the Faraday cup in the target chamber [see Fig. 3(a)]. The physical arrangement was such that for angles greater than +10° the beam cleared the cone supporting slit S_4 and entered the collector. Since the collector was located within the gas and had a +69-V bias, the current I^- actually measured consisted of the incident current I_0 plus a contribution of free electrons from ionized gas atoms. A reasonable assumption, which was checked experimentally, is that the contribution of electrons from ionization is proportional to gas density and incident current, i.e.,

$$I^- = I_0(1 + k_1 n), \tag{5}$$

where k_1 is a constant.

Values of $k_1 n$ were determined from the calibration measurements discussed in Sec. III B and seldom exceeded 15%. Therefore, Eq. (5) was approximated by $I^- = I_0 e^{k_1 n}$. This form, when substituted for I_0 in Eq. (1), allows us to define an effective attenuation constant $\mu = k_1 + 1/n_0$ which includes both beam attenuation and the effect of ionization of the gas. Analysis of the data was then simplified by avoiding separate determinations of k_1 and n_0.

TABLE II. Incident beam parameters.

Item		Value
Current		0.1 – 0.4 μA
Energy resolution[a]		0.08 eV
Nominal diameter[b]		0.5 mm
Angular profile[c]	at 100–400 eV	0.94°
Base width	50 eV	1.5°
Divergence[d]	at 100–400 eV	0.2°
	50 eV	0.5°

[a]Calculated from monochromator parameters.

[b]Approximate beam size expected at the scattering center due to defining apertures S_1 and S_2.

[c]Beam current observed by the analyzer as a function of angle.

[d]One-half the base width minus one-half the angle subtended by the exit aperture S_5 $(a/R = 0.3°)$.

6. *Number Density*

Heat flow from the cathode structure raised the average target-chamber temperature about 30 °C above the temperature of the pressure gauge and created a 20 °C temperature difference between the ends of the chamber. The difference in gauge and chamber temperature necessitated a correction for thermal transpiration[25] in calculating the number density. Since the gauge and chamber were connected by tubulation that was small in diameter compared to the mean free path of the gas, the pressure difference due to thermal transpiration can be expressed in the form

$$P_C/P_G = R, \tag{6}$$

where P_C is the chamber pressure, P_G is the gauge pressure, and R is the thermal transpiration ratio. The ideal value of R for a thin aperture is $R = (T_C/T_G)^{1/2}$, where T_C and T_G and the chamber and gauge temperatures, respectively.

In calculating R and the density n, the chamber temperature was taken as the average of the temperatures at each end. The correction for thermal transpiration when $T_C = 55$ °C and $T_G = 25$ °C reduces the measured cross section by 4.5%. The number density in $(\mu m)^{-3}$ was calculated as

$$n = 1286(T_C/T_G)^{-1/2} P_G$$

with P_B expressed[26] in N/m^2 and temperature in K.

7. *Scattering Angle*

A scattering angle of 5° was chosen both for gen-

eral physical interest in small-angle cross sections and for several practical reasons. At small angles, the scattering intensities were large enough to permit rapid and accurate data acquisition. In addition, at small angles, there was no appreciable contribution from the double scattering process of small-angle inelastic plus large-angle elastic collisions.[26] On the other hand, a 5° angle was adequately larger than the minimum angle of 3.7° for which the entrance aperture remains out of the field of view of the exit apertures.

B. Calibration

1. *Incident Energy*

The incident energy E_0 is believed accurate to within 0.5%. Where necessary, the acceleration potential between the cathode and target chamber was corrected for a contact potential of about −1.3 V. E_0 was determined from the energy of electrons leaving the monochromator and the monochromator target accelerating potential. The mean energy in the monochromator was known from the geometry and deflecting potentials of the hemispheres with an accuracy of about 0.05 eV. The effective monochromator target potential difference was uncertain by an estimated 0.2 V, owing to a limited knowledge of the contact potential.

2. *Transmission Efficiency*

Nearly all of the scattering data were taken with the analyzer operated in the low-resolution full-transmission mode. Full 100% transmission from the target chamber exit aperture [S_5 in Fig. 1(b)] to the analyzer collector was checked in several ways. First, and most importantly, the over-all transmission from the scattering chamber exit aperture S_5 to the analyzer collector was tested by demonstrating that the center portion of each elastic and inelastic loss peak for 5° scattering was flat topped both with respect to energy loss and with respect to changes in all lens and steering voltages in the analyzer. This evidence is regarded as convincing for full transmission through the analyzer.

Second, as an additional test for full transmission from the exit aperture S_5 to the analyzer hemispheres, the primary beam current I_{in} entering the hemispheres was measured by the method described in Sec. III A 3. I_{in} was independent of reasonable changes in all lens and steering voltages in the analyzer, showing that no appreciable current was intercepted on the electrodes between the exit aperture and the analyzer hemispheres. Furthermore, the independence of I_{in} from the influence of excess deflecting voltage between the hemispheres showed that more than 99% of the current incident on the hemispheres was collected; it is assumed that the hemispheres are a nearly perfect collector for elastically reflected electrons.

Third, to test the transmission from the hemispheres to the analyzer collector, the excess deflecting voltage was removed allowing the primary beam to pass through the analyzer exit slit S_6 and reach the collector. The current received at the collector was equal to the hemisphere current I_{in} to within 0.5% for incident energies of 100–400 eV. Below 100 eV, the fraction of current transmitted decreased slightly, reaching about 0.985 at 50 eV. This test demonstrated that the suppressor electrode on the collector [Fig. 2(b)] was effective in retaining secondary electrons produced in the collector.

Finally, for the few cases in which scattering was observed at high resolution, the analyzer constant ΔE_{eff} was determined by measuring I_{in} and the area under the curve $I_F(E)$ for the main beam, where $I_F(E)$ is the current from the analyzer collector measured as a function of the mean energy loss E. ΔE_{eff} was then used to calculate the scattered current from the area under the impact spectrum peaks at 5°. According to the assumptions made in deriving Eq. (4), ΔE_{eff} remains unchanged even though the illumination of the apertures S_4 and S_5 is different at 5° than at 0°, since the exit optics of the analyzer are fixed. Uncertainties of 1–3% in the procedure are introduced by the necessity to measure areas under XY recorder peaks. The correctness of this procedure is borne out by the agreement of the high-resolution data with the low-resolution data (Sec. V B).

3. *Ratio of Scattered to Incident Current*

In determining cross sections, it is sufficient to know the ratio of incident and scattered current, and therefore it was not necessary to have an absolute calibration of current. The scattering chamber current I^- and the current I_{in} to the analyzer hemispheres were measured with a high-impedance digital voltmeter[27] (DVM) shunted by a 10^7-Ω metal-film resistor which had a specified temperature coefficient of $\pm 1.5\times10^{-4}$/°C. The current I_F from the analyzer detector was detected with a vibrating-reed electrometer. The feedback voltage to the base of the input resistor was measured with the DVM. The deposited carbon input resistors used, 10^8 Ω and 10^{11} Ω, had a temperature coefficient of about 0.1%/°C and a measured voltage coefficient of about 0.05%/V. The electrometer was calibrated with respect to the DVM-resistor combination with an estimated accuracy of 0.5%. This estimate is based on two calibrations separated by a six-month interval that overlapped about 70% of the data acquisition. In taking scattering data, the electrometer input was kept below 0.3 V, permitting us to neglect the effect of the voltage coefficient. The laboratory room temperature was

maintained constant to $\pm 1\,^{\circ}$C, which made a temperature correction for resistance unnecessary.

4. *Incident Current*

As discussed above, the observed chamber current I^- differs from the incident current I_0 by the contribution of electrons from ionization in the target gas. It was possible to measure this contribution experimentally as follows. At an observation angle of -15° and with a negative bias on the collector, the observed positive current I^+ was expected to be proportional to the amount of ionization in the gas and was assumed to be

$$I^+ = k_2 n I_0 , \tag{7}$$

where k_2 is a constant. Eliminating I_0 from Eqs. (5) and (7) one obtains

$$nI^-/I^+ \equiv Y = (1 + k_1 n)/k_2 . \tag{8}$$

Indeed, values of Y, at a given energy, depended linearly upon n as predicted by Eq. (8), and a least-squares fit of a straight line to the data was used to calculate k_1 and k_2. Putting k_1 and k_2 back into Eqs. (5) and (7) provided two estimates of I_0 at each operating pressure. These two values of I_0 typically agreed with each other within 2%. The difference is due to, and is a measure of, the imprecision in the measurement of current and number density.

In order to assure that the incident current measured at 15° did not differ significantly from the current at 5°, I_0 was measured over the angular range $10-20^{\circ}$ with no gas admitted to the target. The indicated value of the quantity $[I_0(5^{\circ}) - I_0(15^{\circ})]/I_0(15^{\circ})$ varied from 0 to +2%. If I_0 were to change with the angle, it would be expected to decrease, since the main beam was optimized at zero angle. The corresponding apparent cross section would be biased toward a larger value. In the data analysis, the effects of deviations of $I_0(5^{\circ})$ from $I_0(15^{\circ})$ were assumed to be accounted for in the scatter of the data.

5. *Scattering Geometry*

The size and shape of the exit aperture was measured on an optical comparator at $62.5\times$ magnification by two methods: (a) visual comparison with calibrated reference circles and (b) by micrometer translation of the support bed. The estimated error of the effective diameter was 1%. The width of the exit was measured on a comparator with microscope head to within 1%. The slit length of 0.05 in. insured that the whole height of the incident beam was visible to the exit aperture. The slit and aperture positions relative to the scattering center were determined within 0.005 in.

The uncertainty in angle setting estimated from the tolerances on the internal set of spur gears was about 0.02°.

Backlash in the angular drive was removed by the preload of the flexed metal bellows (30° bend) and the weight of the monochromator. All angular settings were made in a direction which opposed the preload.

A direct check on the accuracy in the angle setting could not be made conveniently. In order to assure that there was no gross error, positioning of the monochromator support bench was demonstrated to be within 0.1° of its expected angular setting over the range of -20° to $+30^{\circ}$.

6. *Oil Density*

Density of the Convoil-20 oil used in the oil manometer was measured at NBS with a precision hydrometer to be 0.8674 g/cm^3 at 24.29 °C. Since the manometer operated at $(25.0 \pm 0.2)\,^{\circ}$C, no correction for temperature was made to the conversion factor of 85.06 N/m^2 per centimeter of oil.

IV. PROCEDURE

Except for a few high-resolution measurements, all scattering data were taken with the analyzer operating in the full-transmission mode. At each data point scattering and calibration measurements, for a given pressure, were made according to the following procedure. After achieving pressure equilibrium, the elastic and $2\,^1P$ energy-loss peaks at 0° and 5° were shown to be flat topped with respect to energy loss and to the adjustment of analyzer lenses and steering voltages.

Immediately before, and again after, taking scattering data the target chamber electron and ion currents I^- and I^+ were recorded. Measurement of the scattered current I_F for elastic, $2\,^1P$, and $2\,^1S$ energy loss were then made at plus and minus 5° angle. This pair of angle settings was usually repeated a second time particularly for $2\,^1P$ scattering where uncertainties in I_F owing to the accuracy of the angle setting were comparable to statistical uncertainties in the signal. At each setting of angle several 10-sec averages of the electrometer output were recorded and averaged. Background was read at 0.6- and 22.2-eV energy loss; these losses are removed from any scattering channels.

Following the remeasurement of scattering chamber currents, the temperature of the hotter end of the target chamber was read relative to an ice bath (0 °C); and at zero scattering angle the primary beam currents to the analyzer spheres and to the analyzer collector were recorded.

Throughout the accumulation of scattering data the target pressure was monitored by the capacitance manometer. The relative pressure readings were normalized to an absolute pressure measurement taken with the oil manometer after the scattering measurement. Without exception, an absolute pressure reading was made at each setting of

gas pressure. The oil manometer was filled with He to bring the capacitance manometer to a nearly null reading and the residual pressure difference was added to the oil reading. Equilibrium was achieved rapidly, essentially within the time required to fill the system. The degree of equilibrium achieved rules out errors owing to leaks or absorption of the gas. With gas in the transfer tubes, the zero of the capacitance manometer was checked by closing the valve to the scattering chamber and opening the bypass line between the inlet ports.

For the purpose of data analysis, the value of scattered current I_F^{obs} at each data point was an average of the $\pm 5^\circ$ readings. The target chamber currents I^- and I^+ and the pressure were an average of the readings taken before and after the scattering measurements. The averages were not necessary for compensating drift which seldom exceeded 0.5% in any of the variables. Number density was derived from the pressure and temperature values according to the procedures discussed above.

V. ANALYSIS AND RESULTS

In general, a one-day run consisted of data at three or more pressures for a fixed incident energy. In this way enough data were available from each run to overdetermine σ, n_0, and I_0. The scattering chamber currents I^- and I^+ provided an estimate of the constants k_1 and k_2 from Eq. (8). No significant variations in these constants were obtained from dif-

TABLE III. Data used in least-squares analysis and results. [a]

E_0	n	Elastic		$2\,^1P$		$e^{-\mu n}$	E_0	n	Elastic		$2\,^1P$		$e^{-\mu n}$
(eV)	(m^{-3})	I_F^{obs}/nI^- (nm^3)	Δ [b] (%)	I_F^{obs}/nI^- (nm^3)	Δ (%)		(eV)	(m^{-3})	I_F^{obs}/nI^- (nm^3)	Δ [b] (%)	I_F^{obs}/nI^- (nm^3)	Δ (%)	
400	637	1.84 [c]	1.5	3.17 [c]	3.6	0.87		628	2.78	1.6	4.93	1.8	0.82
	1418	...	...	2.70 [c]	2.6	0.74	200	0	(3.44	4.2)	(6.09	3.4)	...
	1422	1.54 [c]	2.4	...	...	0.74							
400	565	1.88	0.9	...	...	0.89	150	487	3.42	...	5.23	...	0.83 [e]
	586	...	...	3.39	−2.0	0.88							
	589	1.89	0.0	...	...	0.88	150	0	(4.10	4.8) [d]	(6.27	4.2) [d]	...
	984	1.72	0.7	...	...	0.81	100	563	...	...	3.81 [c]	0.5	0.77
	1001	1.73	−0.2	...	...	0.81		571	3.76 [c]	−0.3	...	...	0.78
400	617	1.90	−1.2	3.34	−1.2	0.87		1460	2.59 [c]	−2.6	2.56 [c]	−1.6	0.51
	934	1.79	−2.2	3.15	−2.1	0.82	100	613	3.57	3.3	3.64	2.6	0.76
	1222	1.69	−2.0	2.95	−1.9	0.77		928	3.11	2.8	3.15	2.4	0.66
400	304	2.02	−0.5	3.52	0.3	0.94		1235	2.74	2.0	2.76	1.3	0.57
	612	1.86	1.0	3.27	1.0	0.88	100	328	4.09	2.3	4.17	2.4	0.86
	911	1.77	−0.2	3.09	0.0	0.82		470	4.06	−3.2	4.14	−3.3	0.81
400	0	(2.14	2.2)	(3.77	3.8) [b]	...		618	3.82	−3.9	3.88	−3.9	0.75
300	615	2.17 [c]	1.4	4.09 [c]	0.3	0.84	100	0	(4.82	5.3)	(4.98	5.0)	...
	1498	1.73 [c]	−0.4	3.15 [c]	−0.1	0.65	75	354	4.62	...	3.00	...	0.89
300	444	2.33	−1.1	4.33	−0.2	0.88		614	4.25	...	2.75	...	0.82
300	0	(2.61	4.6)	(4.93	3.6) [d]	...	75	0	(5.20	9.4) [d]	(3.37	7.2) [d]	...
200	613	...	...	5.07 [c]	−0.6	0.83	50	311	4.23	1.9	1.07	1.2	0.89
	621	2.84 [c]	−0.4	...	...	0.82		461	3.93	3.9	1.00	2.1	0.84
	1372	2.35 [c]	−4.6	4.15 [c]	−3.9	0.66		598	3.72	4.7	0.94	3.6	0.80
200	585	2.82	1.4	5.07	0.2	0.83							
	895	2.56	1.6	4.56	1.2	0.76	50	339	4.37	−2.4	1.08	−1.0	0.88
	1216	2.27	3.3	4.06	3.1	0.69		481	4.25	−4.4	1.06	−3.6	0.84
200	317	3.13	−0.5	5.53	−0.2	0.91		638	3.95	−2.9	0.98	−1.9	0.79
	448	3.05	−2.2	5.38	−1.5	0.87	50	0	(4.81	13.6)	(1.22	9.6)	...

[a] Values in parentheses are results of the least-squares analysis. The percentage errors given are two standard deviations of the mean.

[b] $\Delta = (I_F^{pred} - I_F^{obs})/I_F^{obs}$.

[c] These data were taken in the high-resolution mode, $\Delta E = 0.12$ eV full width at half-maximum (FWHM). Data not so indicated were observed in the low-resolution mode, i.e., with flat-topped peaks of 0.6 eV FWHM.

[d] The error was interpolated from values at adjacent energies in the table.

[e] The value of μ used was interpolated from values at adjacent energies in the table.

ferent runs and, therefore, all of the data at a given incident energy were combined in the final analysis.

A. Method

In order to provide nearly equal weight to the observed scattered current I_F^{obs} at each data point the dependent experimental variable was taken to be IF^{obs}/nI^-. The corresponding predicted current I_F^{pred} was expressed as

$$I_F^{pred}/nI^- = \sigma(W, \theta)(l\Delta\Omega)_{eff} e^{-\mu n} . \quad (9)$$

Equation (9) follows from Eq. (1) when the substitutions I^- for I_0 and μ for $(1/n_0)$ are made for the reasons presented earlier. The method of least-squares estimation of nonlinear parameters[28] was used to determine values of σ and μ that minimized the sum of squared residuals Φ, where

$$\Phi = \sum_{i=1}^{N} [(I_F^{obs} - I_F^{pred})/nI^-]_i^2 ,$$

and i is the running index for the N data points. A Share Library computer code[29] was used for the analysis. Standard errors in the parameters σ and μ were estimated from the last iteration of the nonlinear fitting procedure based on a Taylor series expansion about the converged values.

B. Results

1. *Cross Sections*

Data used in the least-squares analysis are listed in Table III and are grouped together by runs. Elastic and inelastic data entered on the same line were essentially simultaneous measurements and are suitable for determining cross-section ratios. The elastic $2\,^1P$ data were separately fitted, at each energy, without assuming a relationship between the constant μ for each case. The entries in the table for $n=0$ are the least-squares values of $\sigma(l\Delta\Omega)_{eff}$ and their corresponding errors which are two standard deviations of the mean. Values of $\exp(-\mu n)$ from the elastic and $2\,^1P$ analysis did not differ by more than 2% and an average value is given in the table.

TABLE IV. Absolute e^--He cross sections in units of 10^{-18} cm^2/sr, $\theta = 5°$.

E (eV)	Elastic	$2\,^1P$	$2\,^1S$
400	29 (1.5) [a]	50 (3)	3.6 (0.2)
300	35 (2)	65.5 (4)	3.65 (0.2)
200	46.5 (3)	81.5 (4.5)	3.6 (0.2)
150	55.5 (4)	84.5 (5)	3.7 (0.2)
100	65.5 (4.5)	67.5 (4.5)	4.0 (0.25)
75	70.5 (7)	45.5 (4)	4.0 (0.35)
50	65 (10)	16.5 (1.5)	2.9 (0.3)

[a]Total error given in parenthesis is the root sum of squares of twice the standard deviation of the mean and the estimated systematic error of 4.4% (see Table VI).

TABLE V. Relative[a] e^--He cross sections, $\theta = 5°$.

E (eV)	Elastic / $2\,^1P$	$2\,^1S$ / $2\,^1P$
400	0.585	0.0725
300	0.55	0.056
200	0.57	0.044
150	0.66	0.044
100	0.99	0.059
75	1.54	0.0875
50	4.0	0.175 [b]
48	...	0.192 [c]
46	...	0.22 [d]
36	...	0.4 [d]

[a]Including correction for finite angular resolution. Estimated limits of error are 2% 100–400 eV and 3% 50–75 eV (see Sec. V B).

[b]Not corrected for a 2–3% contribution of $2\,^3P$ indicated in Ref. 34.

[c]Taken from Ref. 34.

[d]Taken from Ref. 33.

The close agreement of the high-resolutuion data with the low-resolution data can be regarded as experimental confirmation of the calculations of Kuyatt and Rudd[23] which show that the area under energy-loss peaks is a measure of the total current entering an energy selector with linear dispersion, independent of the size and angular spread of the entering beam (within limits set by physical boundaries).

Entries in Table III do not include corrections for finite angular resolution. The geometry term $(l\Delta\Omega)_{eff}$ is given by $L\Omega(1+n)/\sin\theta$, where n is the correction made to the ideal geometry to account for finite resolution. Nonzero values of n occurred for $2\,^1P$ scattering only and were

E_0(eV)	400	300	200	150
n(%)	+2.5	+2.0	+1.2	+0.7

Elastic and inelastic cross sections derived from Table III and their estimated total error are given in Table IV. Since it is customary to give an overall error assignment to experimental data, we have calculated the estimated total error as the root sum of squares of twice the standard error and the individual estimates of systematic error. This procedure implicitly assumes that the individual sources of error are uncorrelated, and this assumption has not been demonstrated (as is also customary). The $2\,^1S$ cross-section values were calculated using the $2\,^1S/2\,^1P$ cross-section ratios shown in Table V. The percentage error assigned to $2\,^1S$ was the same as that for $2\,^1P$ since the statistical error from the ratio measurements added very little to the total error. The percentage standard errors at the highest energies were smaller than at lower ener-

gies and were consistent with the uncertainty expected on the basis of error in the measurement of pressure and the incident and final scattered currents.

2. *Cross-Section Ratios*

An important and useful test for systematic effects in a given apparatus or between different apparatus is the ratio of scattered currents for different cross sections. A precision in cross-section ratios of the order of 1% can be easily obtained owing to the cancellation of many of the experimental uncertainties. Higher-order pressure effects such as multiple scattering or a difference in the beam attenuation constant $(1/n_0)$ for each cross section are readily discerned.

In the present experiment, cross-section ratios for $2^1S/2^1P$ and for elastic/2^1P scattering were measured with a precision of about 1% for energies of 100 eV and above and with a precision of about 2% at lower energies. The observed ratios are in Table V. Corrections, given above, for the effect of finite angular resolution on the 2^1P scattering were made. Systematic effects were difficult to assess and an additional 1% error was added in estimating the total error to account for residual effects of beam asymmetry.

The degree of precision and the lack of any pressure dependence in the ratio of elastic/2^1P scattering indicate that the value of the attenuation constant μ is the same in each case. This fact was borne out in the data analysis in which the difference in the values of μ for elastic and 2^1P scattering was considerably less than the standard error. Similarly, the ratio of cross sections from the least-squares analysis were expected (and found) to be nearly equal to the directly observed ratios. This can be seen by comparing ratios taken from Table IV with the ratios in Table V.

C. Discussion of Systematic Error

Estimates of systematic errors are summarized in Table VI. Sources of systematic error discussed in this article, but not specifically included in Table VI, are assumed to be small enough to be accounted for in the estimate of standard error based on the scatter in the data.

TABLE VI. Contribution to systematic error in cross-section values.

Source	Estimated limit of error %	Reference
Pressure gauge	1	Sec. V C 1
Uncertainty in number density due to thermal effects	3	Sec. V C 1
Measurement of current	0.5	Sec. III B 3
Relative detector efficiencies	0.3	Sec. V C 2
Geometry ($L\Omega$)	3	Sec. III A 2, Sec. V C 3 and Table I
Beam size and divergence	0.2	Ref. 17
Total (root sum of squares)	4.4	...

1. *Number Density*

The uncertainty in number density due to thermal effects was a result of the nominal 20 °C temperature difference across the scattering chamber and of a 30 °C difference between the mean chamber temperature and the manometer temperature. To within an order of magnitude, the gas atoms had a mean free path of 1 cm and underwent 10^4 collisions during their 0.2-sec residence time in the target chamber. Under these conditions we believe there was adequate temperature and pressure equilibrium in the gas so that the number density and thermal transpiration ratio were determined by the same effective target temperature and that this effective temperature was close to the average of the temperatures at each end of the target. The estimated uncertainty of 3% in number density corresponds to a 20 °C uncertainty in the effective target temperature and is believed to be a conservative estimate. The 3% estimated error also allows for an 0.5% uncertainty in density owing to using the "ideal" value of thermal transpiration ratio R to calculate the pressure difference between the target chamber and manometer, i.e.,

$$P_C - P_G = (1 - R)P_G \ .$$

We assumed a 10% uncertainty in $1 - R$ on the basis of Ref. 30 in which the measured value of R for He in a 2-mm-i.d. glass tube was 10% larger than the ideal value of $R = 0.51$.

Sources of error in the point-contact oil manometer have been examined in detail (Ref. 12) and are dominated by the error in the setting and reading of the micrometers. The error quoted in Table VI is the ratio of the manometer least count (0.15 mTorr) to the nominal mean pressure (15 mTorr).

The fractional decrease in number density due to pumping by the apertures was taken to be $1/4\pi$ times the solid angle subtended by the apertures at a given point in the target. Along the effective path length the above fractional decrease was less than 0.1%.

2. *Current*

The estimated contribution of 0.5% to the error in I_F/I^- due to calibration of the current-measuring instrumentation has been discussed in Sec. III B 3. Errors due to Faraday-cup collection efficiency enter only as the difference in efficiency of the two collectors and this difference was taken to be less than 0.3% based on a maximum of 20% reflection at the bottom of the cup and a maximum probability

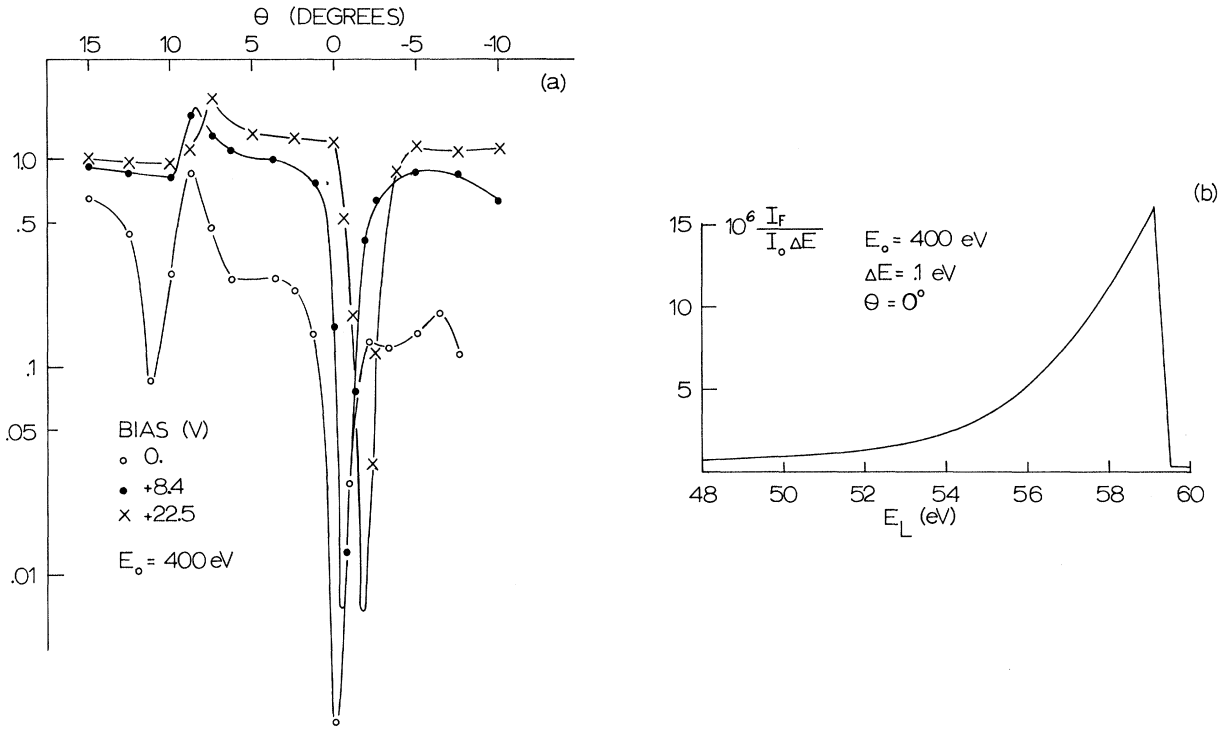

FIG. 5. Experimental data related to tests for secondaries in the incident beam: (a) current received by the target collector, in relative units, as a function of angle setting and the bias on the collector; (b) fraction of the incident current, per unit of energy resolution, received by the analyzer as a function of the apparent energy loss E_L. No gas was being admitted to the target chamber.

of escape of 1.5%.

There is a potential source of systematic error if the measured total current entering the scattering chamber does not represent the effective impact current. This situation can arise if there are secondary electrons in the beam that are removed in energy from the primary beam by more than the energy bandwidth of the spectrometer. The measurement of incident current I_0 accounts for all the incident current including secondaries. If there were a significant number of secondaries, I_0 would be larger than the effective bombarding current and the cross sections obtained would be too small.

In the present apparatus, low-energy secondaries generated in the high-current gun section at slits S_1 and S_2 (Fig. 1) are not a problem; they are removed energetically from the beam by the decelerating lens preceding the monochromator hemispheres. However, there are two possible sources of secondaries between the monochromator hemispheres and the target chamber, namely, the aperture S_3 and the target entrance aperture. In the present apparatus, with the unshielded Faraday collector in the scattering chamber, a direct measurement of the amount of secondaries could not be made. Evidence for believing that their contribution is less than 1% is given below.

The spectrum of secondaries is shown in Fig. 5(b). The area under the curve of about 3×10^{-5} is the fraction in the primary beam of high-energy secondaries seen by the analyzer. The total fraction of high-energy secondaries could not be determined, since their spatial distribution, and hence the collection efficiency of the analyzer could not be determined. However, Fig. 5(b) does demonstrate that the major portion of secondaries will be clustered in energy. This is expected since at the originating surface secondaries primarily have only a few electron volts or less of energy.

Direct retarding measurements on the collector in the target chamber did set an upper limit of 0.5% to the fraction of high-energy secondaries in the beam. The retarding analysis is considered to represent nearly all of the primary beam since the collector, shown in cross section in Fig. 2(a), was 0.25 in. wide and intercepted all but the most extreme rays that could possibly enter the chamber.

A measure of the component of low-energy secondaries generated at the target entrance aperture is taken from the data in Fig. 5(a) for a 400-eV beam. Figure 5(a) gives in relative units the current received at the target collector as a function of angle setting and the positive bias on the collector. The minimum near zero angle is due to the beam passing

through the exit slit and disappearing from view. Current received for nonzero angles is composed of the primary beam and secondaries.

The deep minimum, even with +22 V bias, shows the component of low-energy secondaries in the beam to be less than 1%. The narrow width of the beam confirms the estimate in Table II of a beam width of 0.5 mm or less. Given the beam width and divergence in Table II, the beam does not fill the entrance aperture, which is another reason for believing low-energy secondaries are not generated at the entrance. This conclusion holds down to 100 eV.

Below 100 eV the beam diverges rapidly and secondaries may be produced at the entrance slit. However, a limit on the systematic error from this source cannot be set due to lack of evidence. The error is believed to be small compared to the quoted error. Clearly, further measurements and diagnostics are desirable to increase the accuracy in the very interesting energy range below 100 eV.

3. *Geometry*

By averaging symmetric observations of I_F at $+\theta$ and $-\theta$ to obtain I_F^{obs}, errors in the scattering intensity due to misalignment of the beam with respect to the scattering geometry were cancelled to first order [(See Ref. 17(a) and Sec. III A 2)]. In the present apparatus the asymmetry, defined as the quantity $1-I_F(+\theta)/I_F(-\theta)$, for $2\,^1P$ scattering was about twice that for elastic scattering and was within the range 0 to −5% for 100 eV, −5 to −10% for 75 eV, and −10 to −20% at 50 eV. Above 100 eV the elastic and inelastic asymmetries were less than 2% and could not be clearly distinguished from the uncertainty due to angular setting. The uncertainty in I_F^{obs} due to asymmetry was taken to be one-tenth of the asymmetry itself. This uncertainty was small compared with other errors.

The systematic increase in asymmetry in going to energies below 100 eV was undoubtedly related to the rapid increase in divergence of the primary beam in approaching the low-energy end of the operating range of the apparatus. The asymmetry was pressure dependent, decreasing with increasing pressure, which accounts for the range of values given above. The change in asymmetry with pressure was attributed to smoothing effects in the incident beam owing to nearly zero-angle scattering and creation of positive ions in the gas.

Since the ratio of the elastic/$2\,^1P$ cross sections is a strong function of angle, there was an asymmetry and pressure dependence in the observed ratio of elastic/$2\,^1P$ scattered currents when the ratios at positive and negative scattering angles were compared. However, when value of I_F^{obs} were used to obtain the ratio of elastic/$2\,^1P$ scattering the pressure dependence was reduced by a factor of 10.[31] This tenfold reduction in pressure dependence is evidence of the effectiveness of averaging symmetric observations. In the worst case of 50 eV, the ratio of elastic/$2\,^1P$ scattered currents changed by 0.5% for a change in pressure from 1.3 to 2.6 N/m^2. The variations in cross-section ratio between runs, discussed in Sec. V B, were larger and were consistent with the percentage uncertainty of one-tenth the asymmetry in I_F.

Estimates of systematic error due to beam size and divergence were made using the formulas in Ref. 17 and were quite small. The error in the evaluation of η from Eq. (2) was taken to be 10%. In the worst case, the corresponding error in the apparent cross section would be 0.2%.

VI. DISCUSSION

A. Cross-Section Ratios (5°)

The present elastic/$2\,^1P$ cross-section ratios (Table V) are systematically lower by about 3% than earlier values[32] obtained with substantially the same apparatus. This lowering is attributed to improvements of both the primary beam collimation and the angular symmetry of scattering on opposite sides of the incident beam.

The measured $2\,^1S/2\,^1P$ ratios are in agreement with earlier results[8] when the slit corrections made in the present measurements are taken into account. Table V also lists $2\,^1S/2\,^1P$ ratios below 50 eV measured by Rice, Kuppermann, and Trajmar[33] and by Lassettre, Skerbele, Dillon, and Ross.[34] Their results fit smoothly onto our values. The rapid decrease of the $2\,^1S/2\,^1P$ cross-section ratio for incident energies from 36 to 100 eV is illustrative of the general characteristic of (optical) dipole forbidden transitions to increase more rapidly with energy and reach a peak value at a lower energy than for allowed transitions.

B. $2\,^1P$, $2\,^1S(5°)$

Our results for the $2\,^1P$ differential cross section

TABLE VII. Ratio of experimental to theoretical Born[a] cross sections, $\theta = 5°$.

	$2\,^1P$		$2\,^1S$	
E (eV)	K^2 (a.u.)	Expt / Born	K^2 (a.u.)	Expt / Born
400	0.239	0.905	0.237	0.84
300	0.190	0.885	0.187	0.80
200	0.149	0.825	0.147	0.76
150	0.137	0.78	0.134	0.78
100	0.142	0.685	0.137	0.87
75	0.165	0.585	0.157	0.92
50	0.235	0.375	0.220	0.83

[a]Reference 35.

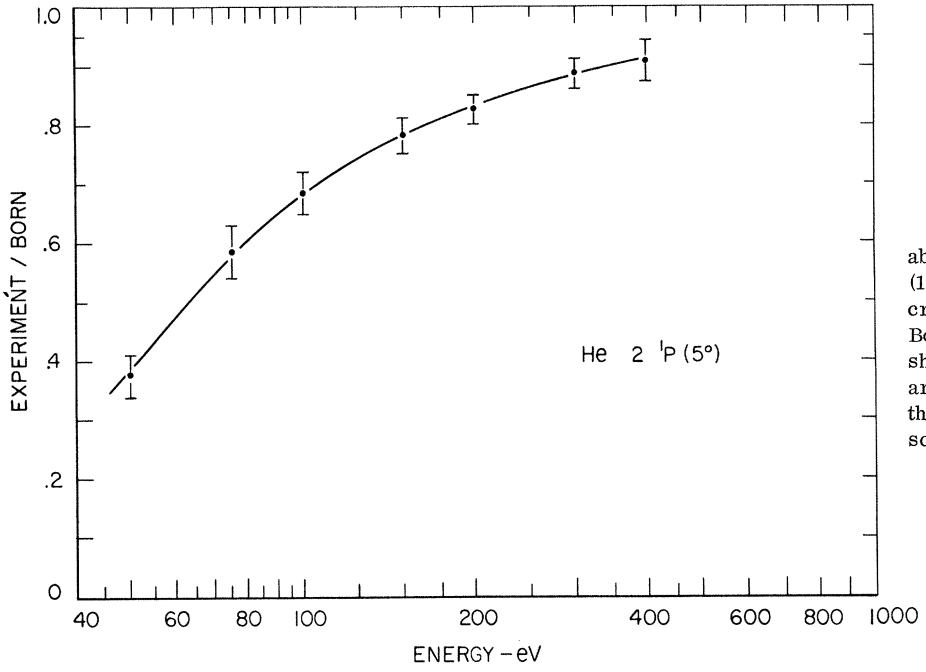

FIG. 6. Comparison of absolute determination of He ($1\,^1S \rightarrow 2\,^1P$) electron impact cross section with theoretical Born values. The errors shown are experimental and are two standard deviations of the mean estimated from the scatter in the data.

relative to the theoretical Born values are listed in Table VII and are shown in Fig. 6. Born cross section values were obtained from the generalized oscillator strengths of Kim and Inokuti[35] which they estimate to be accurate to within 1% of the true Born value. The curve in Fig. 6 suggests that at 400 eV the differential cross section is approaching Born asymptotically. Measurements at higher energies would be of interest in following the approach to the Born cross section and as an added test for systematic error.

In Refs. 8 and 32, cross sections were normalized

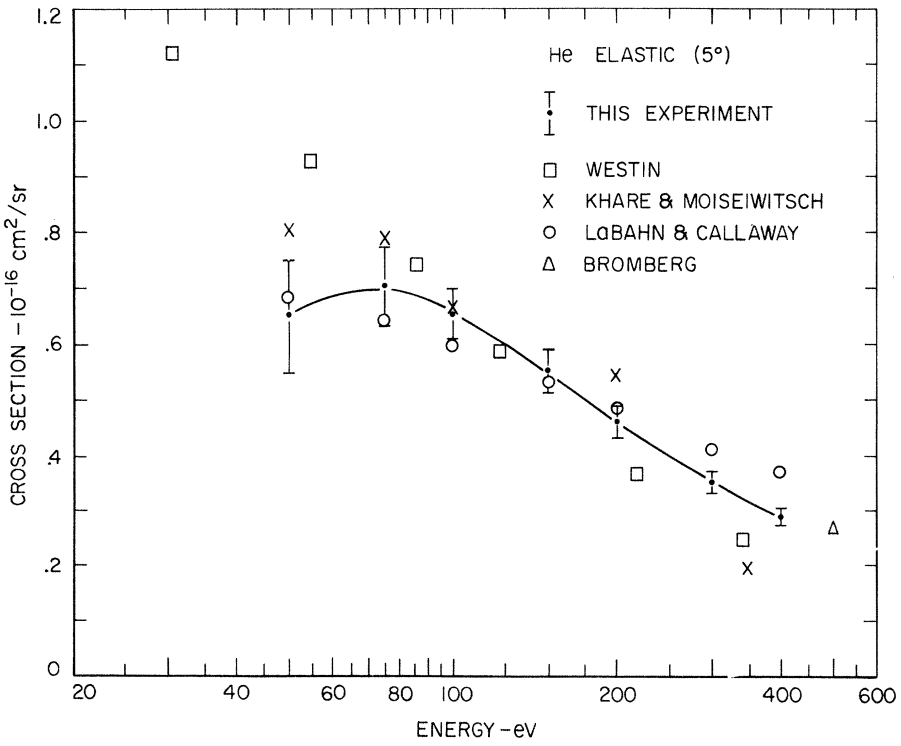

FIG. 7. Results of absolute determination of elastic electron-helium scattering cross section, and comparison with other authors. The errors shown are the root sum of squares of the systematic error and two standard deviations of the mean.

TABLE VIII. Comparison of total $2\,^1P$ cross sections in units of 10^{-18} cm^2.

E (eV)	Vriens *et al.*[a]	Jobe and St. John[b]	Moustafa *et al.*[c]	van Eck and de Jong[d]	Born calculation[e]
$3K$	...	...	1.43	...	1.39
$2K$	...	...	1.88	...	1.93
$1K$	...	...	3.2	3.2	3.3
400	5.5	5.6	5.6	6.0	6.1
300	6.5	6.6	6.4	7.2	7.4
200	7.6	7.9	7.9	8.9	9.4
100	8.7	9.2	9.7	11.7	13.1

[a]Reference 8, renormalized to cross-section values in Table IV. Estimated errors are 3% larger than total error in Table IV.

[b]Reference 42.

[c]Reference 37 renormalized to Born at 1–3 keV.

[d]Reference 43.

[e]Kim and Inokuti, Ref. 35; and Bell *et al.*, Ref. 44.

to the $2\,^1P$ optical oscillator strength value of Schiff and Pekeris[36] $f_0 = 0.276$, by fitting the $2\,^1P$ apparent generalized oscillator strength to an analytic form similar to the right-hand side of Eq. (3), but including higher-order terms. In view of the present results, the elastic, $2\,^1P$, $2\,^1S$, and $2\,^3S$ cross sections in Refs. 8 and 32 should be rescaled.

The differential $2\,^1S$ cross sections relative to theoretical Born values[35] are listed in Table VII. The deviation of 16% at 400 eV and 5° is comparable to the deviation of 10% below Born in the total $3\,^1S$ cross section at 400 eV given in Ref. 37.

C. Elastic (5°)

In Fig. 7 the results for the elastic differential cross section are compared with the theoretical values of Khare and Moiseiwitsch,[38] the "experimental" values of Westin,[3] the theoretical values of LaBahn and Callaway,[39] and the absolute measurement of Bromberg.[40]

Until the recent results in Ref. 39 became available, Khare's theoretical values were the best to compare with, since tabulated[4] phase shifts for $l = 0$, 1, and 2 are not sufficient for comparison at 5°. Khare's result at 350 eV does not include the contribution of polarization, and therefore, it is not surprising that this value lies below our experimental value. The theoretical accuracy is not easily estimated, but the computational inaccuracy was < 1%.

The values quoted for Westin were calculated from the set of phase shifts, $l = 0$ to 6, used by Westin to fit his own absolute cross-section values at 90°, 160°, 170°, and 180° and the angular-dependence data of several other experimenters. Westin's fit was carried out for angles greater than 10°; extrapolation to 5° introduces an additional uncertainty in view of the rapidly increasing importance of high-order phase shifts at small angles. Considering this error and the accuracy of the original data, the difference at 50 eV is reasonable. At higher energies, the cross sections computed from Westin's phase shifts are lower than the present results, as would be expected from the lack of higher-order phase shifts.

The results of LaBahn and Callaway include phase shifts up to $l = 50$ and were calculated using the extended polarization potential approximation.[41] The close agreement with experiment attests to the usefulness of this approximation.

The results of Bromberg[40] for the absolute measurement of differential eleastic scattering at 500 eV are about 8% higher than an extrapolation of our values to 500 eV. Since the estimated error in Bromberg's measurement is 3% and ours is 5%, the experimental results cannot be regarded as inconsistent.

D. Total $2\,^1P$

The total $2\,^1P$ cross section $\sigma_T(2\,^1P)$ is insensitive to the actual shape of the differential cross section, but depends directly on the normalization of $\sigma(2\,^1P,\theta)$. For example, for equal values of f_0 in Eq. (3) the difference in σ_T using either $\alpha^2 = 3.68$ or $\alpha^2 = 3.39$ is about 3%. We have therefore renormalized the values of $\sigma_T(2\,^1P)$ given in Ref. 8 using the present absolute differential cross sections.[42] The results are listed in Table VIII together with other measured and calculated values. Jobe and St. John[45] measured absolute $2\,^1P$ total cross sections by observing the infrared radiation from the $2\,^1P \rightarrow 2\,^1S$ transition. Their absolute error[46] was about 15% and their relative error 4%. The difference of only 1% in absolute magnitude between their values and ours is assumed to be fortuitous.

Moustafa *et al.*[37] and van Eck and de Jong[43] have measured $2\,^1P$ total cross sections by observing the uv radiation from the $2\,^1P \rightarrow 1\,^1S$ transition. Relative values were put on an absolute scale by requiring that a plot of $E\sigma_T(2\,^1P)$ versus $\ln(E)$ have a particular slope; in the Born approximation this slope is simply related to the optical oscillator strength which, in turn, is accurately known from the calculation of Schiff and Pekeris.[36] We have renormalized the measurements of Moustafa *et al.* to agree with theoretical Born values[35] in the region 1–3 keV. The resulting cross sections at lower energies are in good agreement with the present results. The measurements of van Eck and de Jong are intermediate between our results and the theoretical Born values.

ACKNOWLEDGMENTS

The authors thank Dr. S. P. Khare for making numerical values of calculated elastic cross sections available to them. We thank Dr. R. W. LaBahn, J. Callaway, and J. P. Bromberg for making their results available prior to publication. We are grateful to Dr. J. A. Simpson for his encouragement and advice during the course of this work.

†Research supported in part by the Advanced Research Projects Agency of the Department of Defense under the Strategic Technology Office.

*Present address: Joint Institute for Laboratory Astrophysics of the National Bureau of Standards and the University of Colorado, Boulder, Colo. 80302 (Staff member, NBS).

[1]We distinguish an absolute measurement based solely on experimental parameters from normalized cross sections based on measurements relative in angle and/or energy that are referenced to Born or other theoretical values.

[2]The absolute measurement of elastic cross sections, for small and large angles, in atomic and molecular gases and to which inelastic cross sections can be normalized is currently being performed by Lassettre and co-workers. See J. P. Bromberg, Bull. Am. Phys. Soc. 13, 102 (1968); and Ref. 5.

[3]A summary of the experimental work available as of 1947 is found in S. Westin, Kgl. Norske Videnskab. Selskabs Skrifter 2, 1 (1949).

[4]J. Lawson, H. Massey, J. Wallace, and D. Wilkinson, Proc. Roy. Soc. (London) 294, 149 (1966).

[5]E. N. Lassettre, Symposium on Laboratory Measurements of Aeronomic Interest, York University, Toronto, Canada, 1968 (unpublished).

[6]S. Silverman and E. N. Lassettre, J. Chem. Phys. 40, 1265 (1964).

[7]E. N. Lassettre, M. E. Krasnow, and S. Silverman, J. Chem. Phys. 40, 1242 (1964).

[8]L. Vriens, J. A. Simpson, and S. R. Mielczarek, Phys. Rev. 165, 7 (1968).

[9]H. R. Moustafa Moussa, F. J. deHeer, and J. Schutten, in *Fifth International Conference on the Physics of Electronic and Atomic Collisions: Abstracts of Papers*, edited by I. P. Flaks (Publishing House Nauka, Leningrad, 1967), p. 480; L. Vriens, F. J. deHeer, J.v.d. Boss, and H. R. Moustafa Moussa, *ibid.*, p. 491.

[10]C. E. Kuyatt and J. A. Simpson, Rev. Sci. Instr. 38, 103 (1967).

[11]J. A. Simpson and C. E. Kuyatt, J. Appl. Phys. 37, 3805 (1966). Modifications were made in the beam transport optics and resulted in better angular collimation of the incident beam and 100% transmission through the analyzer.

[12]A. M. Thomas and J. L. Cross, J. Vac. Sci. Technol. 4, 1 (1967); Natl. Bur. Std. Tech. Note No. 420, 1967 (unpublished); S. Ruthberg, J. Vac. Sci. Technol. 6, 401 (1969).

[13]C. E. Kuyatt, in *Methods of Experimental Physics*, edited by B. Bederson and W. L. Fite (Academic, New York, 1968), Vol. 7A, p. 1.

[14]E. N. Lassettre and S. A. Francis, J. Chem. Phys. 40, 1208 (1964).

[15]H. R. Worthington, J. N. McGruer, and D. E. Findley, Phys. Rev. 90, 899 (1953).

[16]Data on double scattering in this apparatus has been presented in an earlier publication, G. E. Chamberlain *et al.*, J. Chem. Phys. 47, 4266 (1967). The increase in path length from target entrance to scattering center, 0.8 in. in the present experiment versus 0.3 in. in previous publications, did not appreciably affect the amount of double scattering at larger angles.

[17]G. Breit, H. M. Thaxton, and L. Eisenbud, Phys. Rev. 55, 1018 (1939); C. L. Critchfield and D. C. Dodder, *ibid.* 75, 419 (1949); E. A. Silverstein, Nucl. Instr. Methods 4, 53 (1959). In order to estimate the effects of beam size and divergence using the results of Critchfield and Dodder we put (in their notation) $L = S_0$, $2b = 2c$ = (beam width) = Lx (beam divergence).

[18]One should not be tempted to calculate only the correction to $L/\sin\theta$ for small scattering angles, resulting in a first-order correction term. No such first-order term is given in Eq. (2) owing to cancellation by a term arising from variation in solid angle along the beam path.

[19]In the Born approximation the left-hand side of Eq. (3) is equal to the generalized oscillator strength introduced by H. Bethe, Ann. Physik 5, 325 (1930).

[20]E. N. Lassettre, J. Chem. Phys. 43, 4479 (1965).

[21]L. Vriens, Phys. Rev. 160, 100 (1967).

[22]In the present apparatus, the analyzer is operated at a fixed mean energy and dispersion. An electron-impact spectrum is observed by adding back energy to the electrons after leaving the exit slit S_5. This experiment is concerned only with discrete energy losses. The intrinsic uncertainty in energy loss due to atomic-level widths and kinematics is negligible compared to the spectrometer resolution. Current to the detector for zero energy loss corresponds to elastic scattering at nonzero angles and to a portion of the primary beam at zero angle.

[23]C. E. Kuyatt and M. E. Rudd, Bull. Am. Phys. Soc. 8, 336 (1963); see also Ref. 13, p. 17.

[24]Lens properties were calculated using the analytic expressions in P. Grivet, *Electron Optics* (Pergamon, New York, 1965), p. 167.

[25]L. J. Kieffer and G. H. Dunn, Rev. Mod. Phys. 38, 1 (1966).

[26]The *SI* unit N/m^2 is equal to 7.500 mTorr.

[27]A commercial transistorized unit of 0.01% accuracy, $>10^9\ \Omega$ input impedance, fully floated and guarded input with 140 dB common mode rejection with up to 1000 Ω between either side of input and source.

[28]W. C. Hamilton, *Statistics in Physical Science* (Ronald Press, New York, 1964).

[29]The program used was available as IBM Share Library Distribution No. 1428, and was written by T. Baumeister III and D. W. Marquardt, E. I. DuPont de Nemours and Co., Inc., Wilmington, Del. (unpublished).

[30]Experimental measurements of R and a lengthy discussion of thermal transpiration are found in T. Edmonds and J. P. Hobson, J. Vac. Sci. Technol. 2, 182 (1965).

[31]The invariance of the ratio of elastic/2^1P scattering was additional evidence that there was no constant background of elastic scattering, but did not rule out the unlikely possibility of elastic wall collisions plus elastic collision in the gas. Background from direct wall collisions was checked at zero pressure and found to be negligible.

[32]L. Vriens, C. E. Kuyatt, and S. R. Mielczarek, Phys. Rev. 170, 163 (1968).

[33]J. K. Rice, A. Kuppermann, and S. Trajmar, J. Chem. Phys. 48, 945 (1968).

[34]E. N. Lassettre, A. Skerbele, M. A. Dillon, and K. J. Ross, J. Chem. Phys. 48, 5066 (1968).

[35]Y.-K. Kim and M. Inokuti, Phys. Rev. 175, 176 (1968).

[36]B. Schiff and C. L. Pekeris, Phys. Rev. 134, (1964).

[37]H. R. Moustafa Moussa, F. J. deHeer, and J. Schutten, Physica 40, 517 (1969).

[38]S. P. Khare and B. L. Moiseiwitsch, Proc. Phys. Soc. (London) 85, 821 (1965); S. P. Khare, *ibid.* 86, 25 (1965). Tabulated values were made available

to the authors by Dr. Khare.

[39]R. W. LaBahn and J. Callaway, Phys. Rev. 180, 91 (1969).

[40]J. P. Bromberg, J. Chem. Phys. 50, 3906 (1969).

[41]J. Callaway, R. W. LaBahn, R. T. Pu, and W. M. Duxler, Phys. Rev. 168, 12 (1968).

[42]The renormalization was carried out by setting $\alpha^2 = 3.39$ in Eq. (3) and adjusting f_0 to give agreement with the absolute measurements at 5°. This procedure assumes an angular shape for angles that have not been measured, particularly for the important region of 0° to 5° over which, at 400 eV, the differential cross section makes more than a 50% contribution to the total cross section. Recent experimental measurements [E. N. Lassettre, A. Skerbele, and M. A. Dillon, J. Chem. Phys. 50, 1829 (1969)] over the angular range 2.5°–6° (at 500 eV) show a cross section dependence on K^2 that decreases less rapidly, for small K^2 (0.08 to 0.41), than the angular dependence we assumed. We estimate that the change in the total cross section at 400 eV would be less than 3% if we used the cross-section dependence on small momentum transfer given by Lassettre *et al.*

[43]J. van Eck and J. P. de Jong, Physica 47, 141 (1970).

[44]K. L. Bell, D. J. Kennedy, and A. E. Kingston, J. Phys. B 2, 26 (1969).

[45]J. D. Jobe and R. M. St. John, Phys. Rev. 164, 117 (1967).

[46]J. D. Jobe (private communication).

PHYSICAL REVIEW A VOLUME 2, NUMBER 5 NOVEMBER 1970

Alkali-Alkali Differential Spin-Exchange Scattering. I*

David E. Pritchard, Gary M. Carter†, Frank Y. Chu, and Daniel Kleppner
Physics Department and Research Laboratory for Electronics, Massachusetts Institute of Technology, Cambridge, Massachusetts 02139

(Received 7 April 1970)

We present measurements of differential elastic cross sections for various alkali-alkali pairs, as well as the angular dependence of the probability of electron spin exchange in these collisions. The resolution is sufficient to reveal interference structure in the angular dependence of both quantities. We describe our apparatus, which polarizes one incident beam and analyzes the polarization of the scattered atoms, and discuss the measurement and data-reduction procedures. Results are presented in the range 0.1–0.2 eV for the systems Na-Cs, Na-Rb, Na-K, K-Cs, and K-Rb.

I. INTRODUCTION

Much of our present knowledge of interatomic and intermolecular interactions comes from atomic- and molecular-beam scattering studies. During recent years there has been a steady progression in atomic scattering technique, with a corresponding elaboration of the details of interaction. In the thermal energy range this has been due primarily to increased resolution of velocity and angle. Measurements of the elastic differential cross section now yield very accurate potential curves for systems characterized by a single potential; Pauly's work on alkali–rare-gas systems is a notable example.[1] In more complicated systems there are additional degrees of freedom which govern the interaction. Such systems cannot be adequately described by a single potential, and in order to investigate them experimentally, the scattering apparatus must be able to resolve all the available degrees of freedom.

This paper reports a step in this direction by describing experiments on alkali-alkali interactions which depend on the total spin of the two valence electrons. There are two interaction potentials depending on whether the total spin is 1 or 0, corresponding to the triplet and the singlet state, respectively. Due to the exclusion principle, the singlet interaction is more attractive than the triplet interaction, and the singlet potential lies below the triplet potential at moderate internuclear separations ($5-20\,a_0$). This effect is the result of symmetry, not of direct coupling between the spins. (Direct spin-spin coupling of the valence electrons is sufficiently small to be neglected during the collision.)

The measurements of spin-dependent differential cross sections presented here provide a sensitive measure of the singlet and triplet potentials involved. In experiments without spin-resolution the observed differential cross section [which we call $\sigma_{\text{sum}}(\theta)$] is a weighted average of the cross sections which would be produced by the potentials acting separately. In the present experiments the electron spin of one of the atoms is polarized before the collision and analyzed afterwards, enabling us to measure the probability that scattering through a given angle will be accompanied by exchange of the electron spin, $P_{\text{ex}}(\theta)$. The spin-exchange process results from interference between the singlet and triplet scattering amplitudes and therefore provides a key for separately determining the potentials.

The significance of spin exchange was first ap-